Mon. Not. R. astr. Soc. (1980) 191, 933–949

The effect of a binary companion on a nova outburst

J. MacDonald* *Institute of Astronomy, Madingley Road, Cambridge CB3 0HA*

Received 1979 November 13; in original form 1979 October 18

Summary. We compare two calculations of thermonuclear runaways in solar composition material ($Z = 0.02$) accreted by a $1 M_{\odot}$ white dwarf. We include the interaction of the expanding envelope with a red dwarf companion in only one of the evolutionary sequences. A slow nova results when this binary interaction is included but when it is omitted the outbursts more nearly resemble the very slow novae, like RR Tel and RT Ser.

1 Introduction

Following pioneering observational work of Walker (1954) and Kraft (1964), it is now generally accepted that classical nova outbursts occur in close binary systems, in which a Roche-lobe filling star is transferring mass to a compact companion, most probably a white dwarf. Accretion of hydrogen-rich material by the white dwarf results in formation of a thermally unstable hydrogen shell source (Giannone & Weigert 1967). If the accreted material contains an approximately solar abundance of CNO nuclei, the ensuing thermonuclear runaway gives an outburst that resembles the very slowest (i.e. least energetic) novae (Sparks, Starrfield & Truran 1978; MacDonald 1979; Nariai, Nomoto & Sugimoto 1979). One method of speeding up the outburst is to increase the nuclear energy generation rate by assuming greater than solar abundances of CNO nuclei (Starrfield *et al.* 1972; Starrfield, Sparks & Truran 1974; Starrfield, Truran & Sparks 1978). In this paper we consider, as an alternative, the possibility of tapping the energy of the binary orbit, as discussed in a different context by Paczynski (1976). In Section 2 we show that this binary interaction can be simply modelled by including an extra term in the energy generation rate. In Section 3 we compare two evolutionary calculations of a nova outburst, one with and one without the extra energy generation term. In Section 4 we discuss the relevance of these calculations to an explanation of observed nova outbursts.

2 The binary interaction

The short orbital periods observed in classical nova systems ($\simeq 4$ hr) are consistent with binary separations, S, of order 10^{11} cm. At maximum visual luminosity, novae have spectral

* Present address: The Astronomy Centre, Physics Building, University of Sussex, Falmer, Brighton BN1 9QH.

similarities to A or F supergiants (McLaughlin 1960), and hence have photospheric dimensions of order 5×10^{12} cm. Therefore there is a period in which the Roche-lobe filling star, or secondary, is embedded in the nova envelope. In those novae with expansion velocities less than the relative orbital velocity of the two stars ($\simeq 400\,\mathrm{km\,s^{-1}}$) we expect dynamical friction to play an important role in the evolution of the common envelope (Paczynski 1976).

Let the velocity of outflow be $V_{\rm out}$. The orbital velocity is

$$V_{\rm orb} = (GM/S)^{1/2} \tag{1}$$

where $M = M_1 + M_2$ is the mass of the binary system, M_1 and M_2 are respectively the white dwarf (or primary) mass and the secondary mass.

The accretion radius of the secondary is

$$R_{A,2} = GM_2/(V_{\rm orb}^2 + V_{\rm out}^2 + C_S^2) \tag{2}$$

where C_S is the sound speed in the common envelope in the region of the orbit of the secondary. The secondary fills its Roche-lobe and hence its radius, R_2, is given by (Paczynski 1966)

$$R_2 = S(0.38 + 0.2 \log_{10} q)$$

where $q = M_2/M_1$. (3)

As can be seen from equation (24) in Section 3, C_S is always less than or comparable to $V_{\rm orb}$ and we find $R_A \lesssim R_2$. Since it is essentially due to only the matter that collides with the secondary, the drag force on the secondary, D, is approximately

$$D = \pi R_2^2 \rho V_{\rm orb}^2 \tag{4}$$

where we have assumed $V_{\rm out}^2 \ll V_{\rm orb}^2$.

Dissipation in the envelope is assumed to convert kinetic energy into heat at a rate

$$L_D = DV_{\rm orb} = \pi R_2^2 \rho V_{\rm orb}^3. \tag{5}$$

If this is generated in the torus of radius R_2 centred on the binary orbit, the mean additional energy generation rate is

$$\mathscr{E}_D = L_D/(2S \cdot \pi R_2^2 \rho) = GM/SP, \tag{6}$$

where P is the binary period. For typical values of M and P we find $\mathscr{E}_D \simeq 10^{11}$ erg/g/s.

We have attempted to model the effects of the binary interaction in a spherically symmetric approximation by adding an extra term, $\mathscr{E}_{\rm int}$, to the energy generation rate, neglecting considerations of angular momentum transport in the envelope. The extra term is taken to be

$$\mathscr{E}_{\rm int} = \frac{3\pi}{4} \frac{SR_2}{S^2 + SR_2 + R_2^2} \mathscr{E}_D \quad \text{if} \quad |S - r| \leqslant R_2$$
$$= 0 \quad \text{if} \quad |S - r| > R_2 \tag{7}$$

where r is the distance from the centre of the primary.

The additional factor (of order unity) in equation (7) is to allow for the difference in geometry between the spherically symmetric model and the real situation.

Before discussing the results of the numerical calculations, we note that the binding energy of the nova envelope ($\simeq 10^{46}$ erg) is small compared to the energy of the orbit ($\simeq 10^{48}$ erg). Hence we can take S to be constant throughout the calculation.

3 Numerical calculations

Two evolutionary sequences, A and B, have been computed. In each case we start with a complete spherically symmetric $1M_\odot$ helium white dwarf of luminosity $10^{-3}L_\odot$ and allow it to accrete hydrogen-rich material ($X = 0.7$, $Z = 0.02$) at a rate of $10^{-10}M_\odot$/yr. Some parameters of the initial white dwarf are shown in Table 1. T_{tr} and ρ_{tr} are respectively the temperature and density at the point in the star where the transition between degeneracy and non-degeneracy of the electron gas occurs. More exactly, this point is taken to be where the degeneracy parameter $\psi = 2$. M_e is the mass of material exterior to this point. The computer code is based on that of Eggleton (Eggleton 1971, 1972; Eggleton, Faulkner & Flannery 1973), modified to include hydrodynamics. In this code the total number of mass zones is fixed but the amount of mass in each zone is allowed to change. This allows us to include the complete white dwarf atmosphere in the model with the very fine mass zoning in the outer layers ($\Delta m \simeq 10^{-17}M_\odot$) necessary to give a realistic thermal structure and also allows for the increase in mass due to accretion. A consequence of the changing mass zoning is that the Lagrangian derivatives have to be written

$$\frac{D}{Dt} = \frac{\partial}{\partial t}\bigg|_k - \frac{\partial m}{\partial t}\bigg|_k \frac{\partial}{\partial m} \tag{8}$$

where the subscript k denotes evaluation at constant 'mesh point number'. m is the mass contained within a sphere of radius r.

Table 1. Properties of the 'zero-age' white dwarf.

Mass, M_1	$1.00M_\odot$
Luminosity, L	$1.00\times10^{-3}L_\odot$
Radius, R	5.75×10^{8} cm
Central temperature, T_c	6.26×10^{6} K
Central density, ρ_c	2.81×10^{7} g cm^{-3}
Transition temperature, T_{tr}	3.71×10^{6} K
Transition density, ρ_{tr}	3.25×10^{2} g cm^{-3}
Non-degenerate envelope mass, M_e	$5.75\times10^{-7}M_\odot$
Cooling time, $t_{cool} = C_V MT_c/L$	3.15×10^{9} yr

To ensure numerical stability scalar quantities (density, temperature, etc) are evaluated at the centres of mass zones whereas 'vector' quantities (radius, velocity, luminosity) are evaluated at the edges of mass zones (Sugimoto 1970).

The energy generation rate is taken to be that of the equilibrium pp-chains and the equilibrium CNO-cycle. The time independent Bohm–Vitense theory of fully developed convection as formulated by Baker & Temesvary (1966) is used, together with the diffusion approximation to radiative transfer.

The extra energy generation rate, $\mathscr{E}_{int}$, given by equation (7) was included in sequence B but not in sequence A. The binary separation, S, was taken to be 10^{11} cm. We further assume

Table 2. Properties of the secondary and the orbit in sequence B.

Mass, M_2	$0.46\,M_\odot$
Radius, R_2	3.10×10^{10} cm
Binary period, P	3.97 hr
Binary separation, S	1.00×10^{11} cm
Orbital velocity, $V_{\rm orb}$	440 km s^{-1}
Interaction energy generation rate, $\mathscr{E}_{\rm int}$	7.07×10^{10} erg g^{-1} s^{-1}

that the secondary is an unevolved main sequence star with radius related to mass by (Whyte 1978, private communication)

$$R_2/R_\odot = 0.9(M_2/M_\odot)^{0.9}. \tag{9}$$

The requirement that the secondary fills its Roche-lobe gives $M_2 = 0.46\,M_\odot$. Other derived quantities for the secondary are given in Table 2.

Since the binary interaction does not 'switch on' until $R_1 = S - R_2 = 6.9\times10^{10}$ cm, the early stages of sequences A and B are identical. We shall first briefly describe the evolution of sequence A.

If the accretion rate is low enough the non-degenerate envelope can adjust to the gravitational energy source resulting from the accretion. The critical accretion rate for this to occur can be estimated as follows:

In the absence of accretion, the equations of radiative energy transfer and hydrostatic equilibrium for the non-degenerate envelope can be integrated if the opacity law is of form

$$\kappa = \kappa_0 \rho^\lambda T^\nu \tag{10}$$

to give

$$T = KP^\nabla \tag{11}$$

where

$$\nabla = \frac{\lambda+1}{4+\lambda-\nu} \tag{12}$$

and

$$K = \left[\frac{3}{16\pi}\,\frac{4+\lambda-\nu}{\lambda+1}\,\frac{\kappa_0 L}{acGM}\left(\frac{\mu}{\mathscr{R}}\right)^\lambda\right]^{1/(4+\lambda-\nu)} \tag{13}$$

where M is now the white dwarf mass and μ is the mean molecular weight of the envelope material.

Assuming equation (11) still holds with L constant, in the presence of accretion at rate F, the additional total energy generation in the envelope due to accretion is

$$\begin{aligned} L_{\rm acc} &= \int_{M-M_{\rm e}}^{M} -T\left.\frac{dS}{dt}\right|_m dm \\ &= \frac{1}{\nabla}\left(1-\frac{5\nabla}{2}\right)\frac{\mathscr{R}}{\mu}FT_{\rm tr}. \end{aligned} \tag{14}$$

For a Kramers' opacity law ($\lambda = 1$, $\nu = -3.5$) appropriate to a white dwarf envelope, $\nabla = 4/17$.

Conduction by the degenerate electrons is very efficient at transferring heat in the white dwarf core and hence it is a reasonable approximation to take $T_{tr} = T_c$, so that

$$\frac{L_{acc}}{L} \simeq \frac{7}{4}\frac{\mathscr{R}}{\mu}F\frac{T_c}{L} = \frac{7}{6}\frac{\mu_{ion}}{\mu}\frac{t_{cool}}{t_{acc}}. \tag{15}$$

We see that accretional heating in the envelope can be ignored only if

$$\frac{\mu_{ion}}{\mu}t_{cool} \ll t_{acc} \tag{16}$$

where $t_{acc} = M/F$ is the accretion time-scale. Inserting appropriate values of μ_{ion} and μ for helium we see that the gravitational energy release in the envelope will be important in sequence A. In contrast to the findings of Giannone & Weigert (1967) for a $0.5\,M_\odot$ white dwarf accreting at a high rate, the evolution of the accreted material is not adiabatic.

This can be seen from Fig. 1, which is the ($\log T - \log P$) diagram for a point in the shell source. The arrows show the direction of evolution. The particular point chosen is $3.25 \times 10^{-6} M_\odot$ from the base of the accreted material, and is the point where the maximum shell source temperature occurs. During the early accretion stage $(d \ln T/dt)/(d \ln P/dt) \simeq 0.16$ is much less than the adiabatic gradient ($\nabla_a \simeq 0.4$). Instead of evolving adiabatically, the accreted material reaches a 'quasi-equilibrium' in which the thermal energy generation rate is

$$\mathscr{E}_{th} \simeq FT\frac{\partial S}{\partial m} \simeq C_P T(\nabla_a - \nabla)\frac{F}{M-m} \tag{17}$$

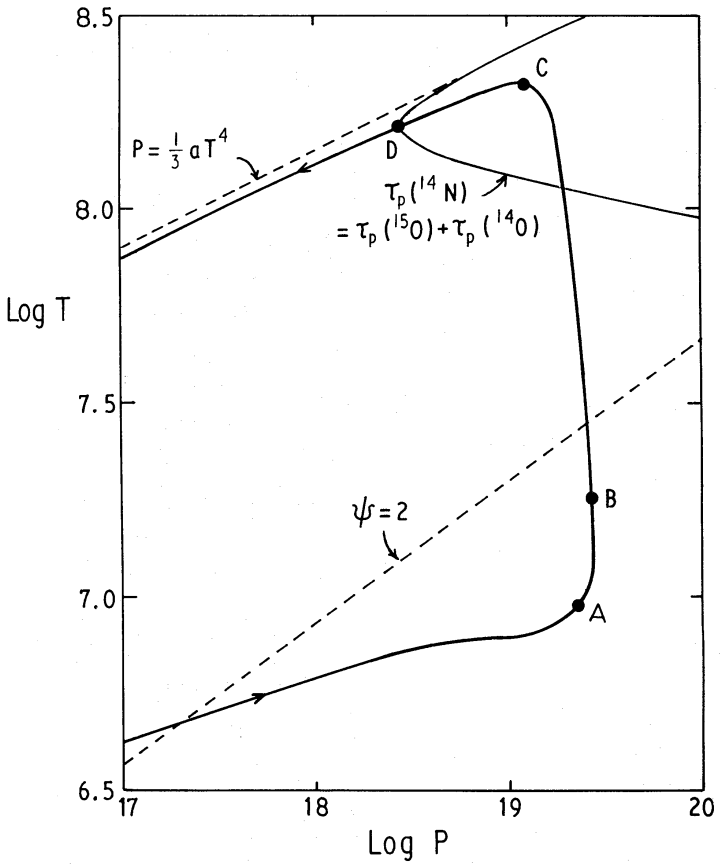

Figure 1. The thick solid line shows the evolution in the ($\log T$–$\log P$) plane of a point in the shell source. The transition from degeneracy to non-degeneracy of the electrons is shown by the lower broken line. The thin solid line separates the regions of the 'fast' and 'slow' CN-cycles. The points A, B, C, D are discussed in the text.

where now

$$\nabla = \frac{d \ln T}{d \ln P}$$

and

$$\nabla_a = \left.\frac{\partial \ln T}{\partial \ln P}\right|_S.$$

This behaviour was also found in a third calculation (sequence C) in which a $1M_\odot$ white dwarf of luminosity $10^{-1}L_\odot$ was accreting at $10^{-7}M_\odot$/yr. For these parameters, $\mu_{ion}t_{cool}/\mu t_{acc} \simeq 50$, is much greater than in sequence A, for which $\mu_{ion}t_{cool}/\mu t_{acc} \simeq 1$.

The difference in behaviour can be attributed to the difference in treatment of accretion. Giannone & Weigert (1967) add mass by introducing additional mass zones, which are forced to evolve adiabatically on the first time-step. If the added zones have a long enough thermal time-scale, as is the case in the calculations of Giannone and Weigert, they prevent the underlying material from cooling and hence the accreted material will continue to evolve adiabatically. Our method of adding mass allows the accreted material to cool and hence the evolution is not necessarily isentropic. We believe our method of accretion to be the more physically realistic in the framework of the spherical approximation. Equation (17) is valid only in accreted material. Non-degenerate material present before the start of accretion will evolve adiabatically if the thermal time-scale of the envelope is much greater than t_{acc}. This occurs in sequence C and a temperature inversion develops. In sequence A, $t_{cool} \simeq t_{acc}$, and hence this region does not evolve adiabatically. However, $(d \ln T/dt)/(d \ln P/dt)$ is greater than in the newly accreted material.

The envelope of sequence A is radiative and hence from equation (17) we see that $\mathscr{E}_{th} > 0$ in the accreted material. Therefore the white dwarf increases in luminosity during the accretion stage. It also expands slightly because the mean molecular weight of the accreted material is less than that of the original (helium) white dwarf and so a lower density is required to give the same pressure.

As the hydrogen-rich material is accreted the temperature at its base increases. Eventually conditions are right for the onset of nuclear burning, which we take to be when the total nuclear energy generation rate is equal to the photospheric luminosity. This occurs in sequence A when M_a, the accreted mass, is $1.08 \times 10^{-4}M_\odot$ (point A in Fig. 1) and is due to the pp-chains in this case. As shown by Giannone & Weigert (1967) this nuclear burning is unstable, either because it is in degenerate material (as in sequence A) or because of the thin shell instability (Schwarzschild & Härm 1965) if the onset of nuclear burning is in non-degenerate material.

If there was no conduction into the core, the instability would develop on a nuclear time-scale

$$t_{nuc} = C_p T_{ss}/\mathscr{E}_{nuc} \tag{18}$$

where T_{ss} and $\mathscr{E}_{nuc}$ are the peak temperature and nuclear energy generation rate in the shell source respectively. At the onset of nuclear burning in sequence A, $t_{nuc} = 3.34 \times 10^5$ yr is shorter than the time taken to accrete the envelope, 1.08×10^6 yr.

However, the temperature in the shell source is low enough for electron conduction to be important. The thermal time-scale in the shell source,

$$t_{th} \simeq \frac{3\kappa C_p (M_a)^2}{64\pi^2 acr^4 T_{ss}^3} \tag{19}$$

is 2.58×10^5 yr, i.e. less than t_{nuc}. Hence conduction slows the thermonuclear runaway and allows further accretion to take place. The total mass accreted is $1.39 \times 10^{-4} M_\odot$.

As T_{ss} increases, the temperature gradient above the shell source also increases until $\nabla = \nabla_a$. Convection then sets in. This occurs in sequence A when $T_{ss} = 2.18 \times 10^7$ K (point B in Fig. 1). As T_{ss} continues to increase, the convection zone grows outwards, also on a nuclear time-scale.

From Fig. 1 we see that T_{ss} increases at nearly constant pressure until radiation pressure becomes important and causes the envelope to expand. A rough estimate of T_{max}, the temperature at which this occurs, is obtained by equating radiation pressure with the pressure at the base of the accreted material.

$$\tfrac{1}{3} a T_{max}^4 \simeq P_a \simeq \frac{GMM_a}{4\pi R^4}. \tag{20}$$

For sequence A this gives $T_{max} = 3.28 \times 10^8$ K. The value found in the numerical calculations, $T_{max} = 2.11 \times 10^8$ K (point C in Fig. 1) is less than this, not only because the envelope has expanded during the evolution, decreasing P_a, but also because gas pressure is not completely negligible.

At temperatures greater than about 10^8 K the energy generation rate is dominated by the 'fast CN-cycle' (Caughlan & Fowler 1972) in which the proton capture time-scales are less than the β-decay time-scales. In particular the $^{13}N(p, \gamma)^{14}O$ reaction is faster than the $^{13}N(, \beta^+\nu)^{13}C$ reaction. Since the reaction $^{14}O(p, \gamma)^{15}F$ does not occur (Caughlan & Fowler 1972) there is a build up of ^{14}O. Similarly the $^{15}O(p, \gamma)^{16}F$ does not occur and hence the CN-cycle time is governed by the β-decay time-scales of ^{14}O and ^{15}O. This sets an upper limit on the equilibrium CN-cycle energy generation rate of

$$\mathscr{E}_{nuc,max} = 7 \times 10^{15} Z_{CN} \text{ erg g}^{-1} \text{ s}^{-1} \tag{21}$$

where Z_{CN} is the abundance by weight of carbon and nitrogen. For solar system abundances $\mathscr{E}_{nuc,max} \simeq 10^{14}$ erg g^{-1} s^{-1}. The domains in the ($\log X\rho$–$\log T$) plane in which the CNO cycle rate is determined by the various reactions is shown in Fig. 2. Also shown (by a dashed line) is the run of $\log X\rho$ against $\log T$ in the envelope of sequence A at the time of maximum shell source temperature.

As pointed out by Starrfield *et al.* (1972), this limit on $\mathscr{E}_{nuc}$ set a limit on the expansion velocity at the time of peak T_{ss}. By considering the energy balance of the now completely convective envelope it can be shown that

$$\mathscr{E}_{nuc,max} \simeq \frac{GM}{R^2} V_{exp}. \tag{22}$$

For sequence A, this gives $V_{exp} \simeq 3 \times 10^5$ cm s^{-1}. Again because of the envelope expansion, the value found in the numerical calculations, 5.9×10^5 cm s^{-1}, is higher.

Contemporaneously with the maximum in T_{ss}, the convection zone extends to the photosphere. This results in a dramatic rise in luminosity from a minimum of $3.61 \times 10^{-3} L_\odot$ to $10^4 L_\odot$, 2.19 hr later. A consequence of the slow expansion is that the photospheric temperature rises dramatically to a maximum of 2.04×10^5 K. The nova is a bright UV source at this stage. After the initial rapid rise, the bolometric luminosity continues to increase but less dramatically, reaching a plateau of $2 \times 10^4 L_\odot$ after a further 4.00 day. Further expansion of the photosphere now causes the photospheric temperature to drop, the bolometric correction decreases and hence the visual luminosity increases.

Since it is essentially the rate of expansion of the envelope that determines the rise time of the nova it is worth considering in more detail how the envelope structure evolves. After

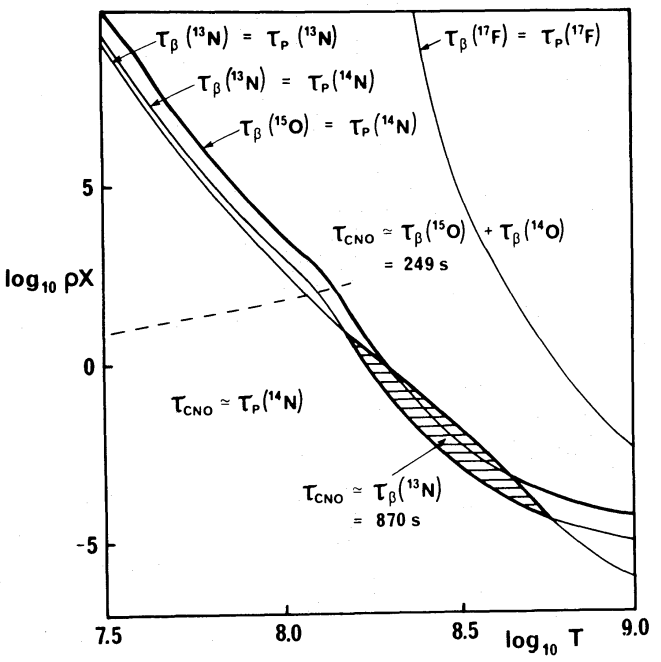

Figure 2. The thick solid lines separate the domains of the (log T–log $X\rho$) plane in which the various reactions of the CNO-cycle determine the nuclear energy generation rate. τ_β is the β-decay time-scale and τ_p is the lifetime against proton capture. The broken line shows the run of log $X\rho$ against log T in the envelope of sequence A at the time of maximum shell source temperature.

the time of maximum photospheric temperature, radiation provides the dominant contribution to the pressure throughout the accreted envelope. Also electron scattering is the main source of opacity. The envelope structure consists of a sub-photospheric radiative region overlying a convective region that extends down to the shell source. In the radiative region the luminosity is uniform and hence β, the ratio of gas pressure to total pressure is also uniform in this region. In the convection zone that persists above the shell source, $\nabla = \nabla_{ad} \simeq 0.25$ for small β. Hence the complete envelope structure can be approximated by a polytrope of index $n = 3$, in which

$$P = \left(\frac{\mathscr{R}}{\mu}\right)^{4/3} \left(\frac{3}{a}\right)^{1/3} \left(\frac{1-\beta}{\beta^4}\right)^{1/3} \rho^{4/3} \tag{23}$$

μ is also uniform by virtue of the convective mixing.

Integrating the equation of hydrostatic equilibrium (dynamic effects are not yet important) gives

$$\frac{P}{\rho}\frac{1}{\beta}\frac{\mathscr{R}T}{\mu} = \frac{GM}{4}\left(\frac{1}{r} - \frac{1}{R_e}\right) \tag{24}$$

where R_e is the outer radius of the envelope.

The total mass of the envelope, M_{env}, is related to β by

$$M_{env} = 4\left(\frac{GM}{4}\right)^3 \left(\frac{\mu}{\mathscr{R}}\right)^4 \frac{a}{3}\frac{\beta^4}{1-\beta} I(0,4;\epsilon,1) \tag{25}$$

where

$$I(m,n;a,b) = \int_a^b z^{m-1}(1-z)^{n-1}\,dz \tag{26}$$

$$= B_b(m,n) - B_a(m,n) \tag{27}$$

and

$$B_x(m,n)=\int_0^x z^{m-1}(1-z)^{n-1}\,dz \tag{28}$$

is the Incomplete Beta Function (Abramowitz & Stegun, 1972, p. 263).

In equation (25), $\epsilon = R_i/R_e$ where R_i is the 'inner radius' of the envelope, i.e. the radius of the shell source. Also

$$I(0,4;\,\epsilon,1)=-\frac{11}{6}-\ln\epsilon+3\epsilon-\frac{3}{2}\epsilon^2+\frac{1}{3}\epsilon^3. \tag{29}$$

From equations (25) and (29) we see that as the envelope expands (i.e. ϵ decreases), β decreases slowly. Since

$$\beta=1-\frac{L_{\rm rad}}{L_{\rm ed}} \tag{30}$$

where $L_{\rm rad}$ and $L_{\rm ed}$ are the radiative and Eddington luminosities respectively, we see that $L_{\rm rad}$ and hence the photospheric luminosity of the star increases slightly as the star expands.

The internal energy of the envelope is

$$U=\int_{M-M_{\rm env}}^{M}\left(\frac{3}{2}\frac{\mathscr{R}}{\mu}T+\frac{aT^4}{\rho}\right)dm=\frac{3}{8}(2-\beta)\cdot\frac{GMM_{\rm env}}{R_i}\,\epsilon\frac{I(-1,5;\epsilon,1)}{I(0,4;\epsilon,1)} \tag{31}$$

and the binding energy is

$$-V=\int_{M-M_{\rm env}}^{M}\frac{GM}{r}\,dm=\frac{GMM_{\rm env}}{R_i}\,\epsilon\cdot\frac{I(-1,4;\epsilon,1)}{I(0,4;\epsilon,1)}. \tag{32}$$

For small ϵ, ($\lesssim 0.03$) we find

$$U\simeq {}^3\!/_8(2-\beta)\frac{GMM_{\rm env}}{R_i}\left\{\ln\alpha-\frac{11}{6}\right\}^{-1} \tag{33}$$

$$-V\simeq\frac{GMM_{\rm env}}{R_i}\left\{\ln\alpha-\frac{11}{6}\right\}^{-1} \tag{34}$$

where $\alpha = 1/\epsilon$.

The global energy balance for the envelope is approximately

$$\frac{d}{dt}(U+V)=L_{\rm nuc}-L_* \tag{35}$$

where $L_{\rm nuc}$ is the total nuclear energy generation rate (including neutrino losses) and L_* is the bolometric luminosity of the star (energy losses into the core are negligible). Equation (35) is valid provided the total kinetic energy is negligible, and can be re-written

$$\frac{d\alpha}{dt}=(L_{\rm nuc}-L_*)\Big/\frac{d(U+V)}{d\alpha} \tag{36}$$

which gives the velocity in terms of $L_{\rm nuc}$, L_* and R_e.

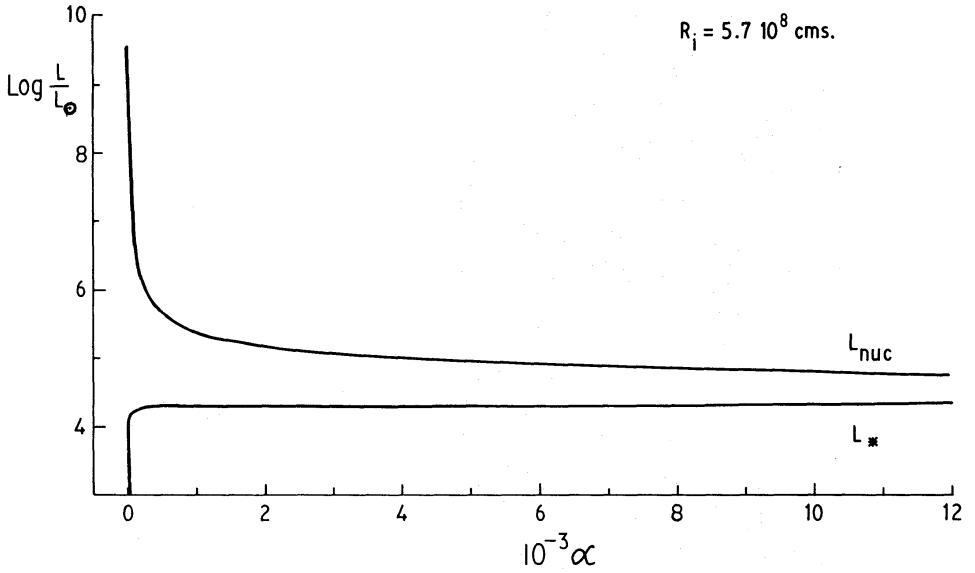

Figure 3. Graph of nuclear luminosity, L_{nuc}, and photospheric luminosity, L_*, against dimensionless radius, α, for sequence A. R_i is defined in the text.

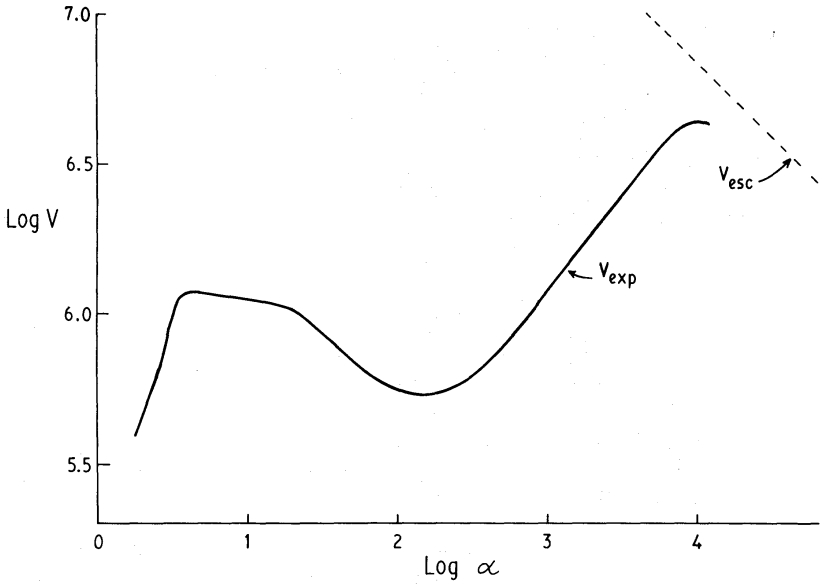

Figure 4. Graph of expansion velocity, V_{exp}, against dimensionless radius, α, for sequence A. The escape velocity, V_{esc}, is shown by the broken line.

At the time of maximum shell source temperature, $L_{nuc} = 3.53 \times 10^9 L_\odot$ and the mean nuclear energy generation rate is 4.98×10^{13} erg g^{-1} s^{-1}. Hence the fast CN-cycle is operating in about half the accreted material. As α increases, L_{nuc} initially drops so rapidly that the expansion velocity, V_{exp}, decreases. As α increases further, L_{nuc} drops less rapidly and V_{exp} increases again. This behaviour can be seen in Figs 3 and 4 which are graphs of L_{nuc} and V_{exp} against α.

When T_{ss} has dropped sufficiently for the β^+-decays to be faster than the proton captures, we can approximate $\mathscr{E}_{nuc}$ by

$$\mathscr{E}_{nuc} = \mathscr{E}_0 \rho T^\eta \tag{37}$$

for some $\mathscr{E}_0$ and η.

This occurs in sequence A when $T_{ss} = 1.65 \times 10^8$ K, and $\rho = 45.6\,\mathrm{g\,cm^{-3}}$ (point D in Fig. 1). The nuclear luminosity is now approximately

$$L_{nuc} = M_{env}\mathscr{E}_{nuc,a}(1-\epsilon)^{-\eta-3}\epsilon^{\eta+3}\frac{I(-\eta-3,\eta+7;\epsilon,1)}{I(0,4;\epsilon,1)} \tag{38}$$

where $\mathscr{E}_{nuc,a}$ is the nuclear energy generation rate at the base of the accreted material.

From equations (23), (24) and (38) we find for small ϵ, that

$$L_{nuc} \simeq M_{env}\mathscr{E}_0 \cdot \frac{\beta^{4+\eta}}{1-\beta}\left(\frac{\mu}{\mathscr{R}}\right)^{4+\eta}\frac{a}{3}\left[\frac{GM}{4R_i}\right]^{3+\eta}\frac{1}{\eta+3}\left\{\ln\alpha - \frac{11}{6}\right\}^{-1}. \tag{39}$$

Finally from equations (25) and (29) we have

$$L_{nuc} \propto \left\{\ln\alpha - \frac{11}{6}\right\}^{-(2+\eta/4)} \tag{40}$$

Whilst $L_{nuc} \gg L_*$ we find from equations (33), (34) and (36) that

$$\frac{d\alpha}{dt} \propto \alpha\left\{\ln\alpha - \frac{11}{6}\right\}^{-\eta/4}. \tag{41}$$

The rhs is minimum when

$$\alpha = \alpha_{min} \equiv \exp\left\{\frac{11}{6} + \frac{\eta}{4}\right\}. \tag{42}$$

For the conditions in sequence A, η is typically 12 and hence the expansion velocity starts to increase again when $\alpha \simeq 130$ (see Fig. 4), reaching a maximum of $40\,\mathrm{km\,s^{-1}}$ at $R_e = 6 \times 10^{12}$ cm.

Since the bolometric luminosity is almost constant at $\simeq 2 \times 10^4 L_\odot$, the maximum in visual luminosity occurs when the bolometric correction is least, i.e. when the effective temperature $T_{eff} \simeq 6000$ K. This corresponds to photospheric radius, $\simeq 9 \times 10^{12}$ cm. Hence at maximum visual luminosity, $\alpha \simeq 10^4$. From equations (41) and (42) with $\eta = 12$, we see that the velocity at the time of maximum light is only about seven times the velocity when $\alpha = \alpha_{min}$.

This has the important consequence that the expansion velocity at maximum visual luminosity can be no greater than about seven times the expansion velocity at the time of maximum T_{ss}, unless some of the assumptions in the $n = 3$ polytrope model break down.

One assumption that is violated is that the opacity is always due to electron scattering. When the effective temperature drops to $\simeq 10^4$ K, recombination of hydrogen occurs. Initially this causes an increase in opacity above the Thomson value and hence an increase in acceleration. Further cooling results in nearly complete recombination and a sharp drop in opacity. As a consequence, L_{ed} decreases and the material loses its radiation pressure support, and decelerates. Material deeper in the envelope is still being accelerated and hence a shell of material forms. At the end of the calculations in sequence A, the expansion velocity is still less than escape velocity ($\simeq 50\,\mathrm{km\,s^{-1}}$) and hence it is not clear whether mass loss will occur. The evolution may possibly proceed in the manner found by Sparks *et al.* (1978), in which gas pressure becomes important and continues the expansion.

However, it is clear from our numerical calculations that at the time of maximum visual luminosity the expansion velocity is much less than observed in slow novae (typically $300\,\mathrm{km\,s^{-1}}$).

A second assumption of the $n = 3$ polytrope model is that the only source of energy to drive the expansion is nuclear burning. It was shown in Section 2 that dynamical interaction with the binary companion is also an important energy source. This interaction was included in sequence B, which is identical to sequence A until the start of the interaction, i.e. until $R_1 = S - R_2 = 6.9 \times 10^{10}$ cm. The mean nuclear energy generation rate at this time,

$$\bar{\mathscr{E}}_{\rm nuc} = L_{\rm nuc}/M_{\rm env} = 5.62 \times 10^{10} \text{ erg g}^{-1} \text{ s}^{-1}$$

is less than $\mathscr{E}_{\rm int} = 7.07 \times 10^{10} \text{ erg g}^{-1} \text{ s}^{-1}$. Hence we see that the binary interaction is important at a fairly early stage of the evolution, i.e. on the rise to maximum visual luminosity. As $\mathscr{E}_{\rm int}$ is independent of density the total luminosity produced by the interaction is solely determined by the amount of material in the interaction zone around the binary orbit, i.e. between radii $S - R_2$ and $S + R_2$. Denoting this mass by $M_{\rm int}$, we have

$$L_{\rm D} = M_{\rm int}\, \mathscr{E}_{\rm int}. \tag{43}$$

The binary interaction becomes important dynamically when $L_{\rm D} \simeq L_{\rm ed}$, i.e. when

$$M_{\rm int} \gtrsim L_{\rm ed}/\mathscr{E}_{\rm int} \equiv M_{\rm dyn}. \tag{44}$$

For sequence B, $M_{\rm dyn} = 10^{-6} M_\odot$, corresponding to a density in the interaction zone of $\rho_{\rm dyn} = 5 \times 10^{-7} \text{ g cm}^{-3}$. If the density in the interaction zone becomes greater than $\rho_{\rm dyn}$, the total luminosity becomes greater than $L_{\rm ed}$ and radiation pressure causes an expansion, limiting the density to near $\rho_{\rm dyn}$.

In sequence A the maximum density at $r = S = 10^{11}$ cm is $3.96 \times 10^{-6} \text{ g cm}^{-3}$, occurring when $\alpha = 2750$. Since this is greater than $\rho_{\rm dyn}$, we see that the binary interaction must be taken into account.

It has the effect of increasing the expansion velocity and, therefore, the rate of increase of visual luminosity. This can be seen in Figs 5 and 6 in which the light curves of sequences A and B are compared and also in Fig. 7 in which $V_{\rm exp}$ is plotted against the dimensionless radius α. The upper and lower curves in Figs 5 and 6 are the bolometric and visual luminosity respectively. The oscillations in the light curve of sequence B are not physical but are due to the coarseness of the mesh spacing in the interaction zone.

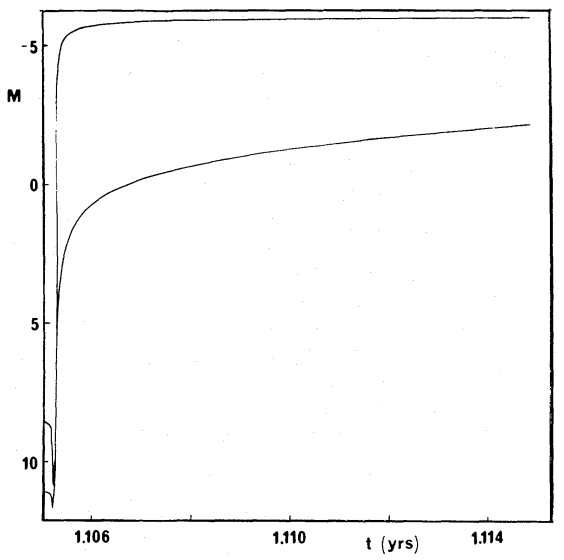

Figure 5. Part of the light curve of sequence A for comparison with sequence B (see Fig. 6). The upper and lower curves are, respectively, bolometric and visual magnitude against time, t.

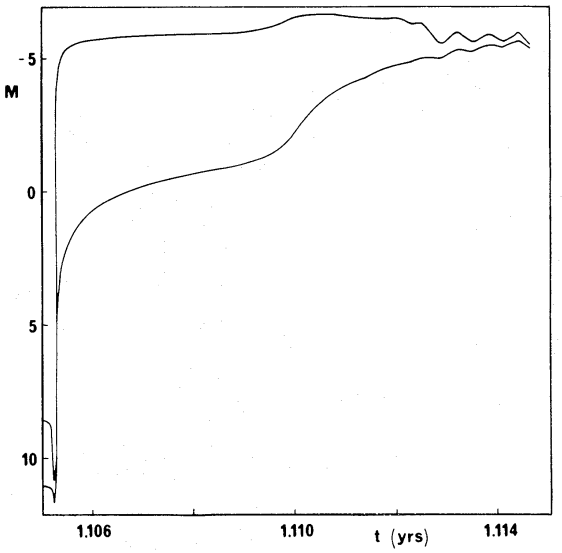

Figure 6. The light curve of sequence B. The curves are as for Fig. 5.

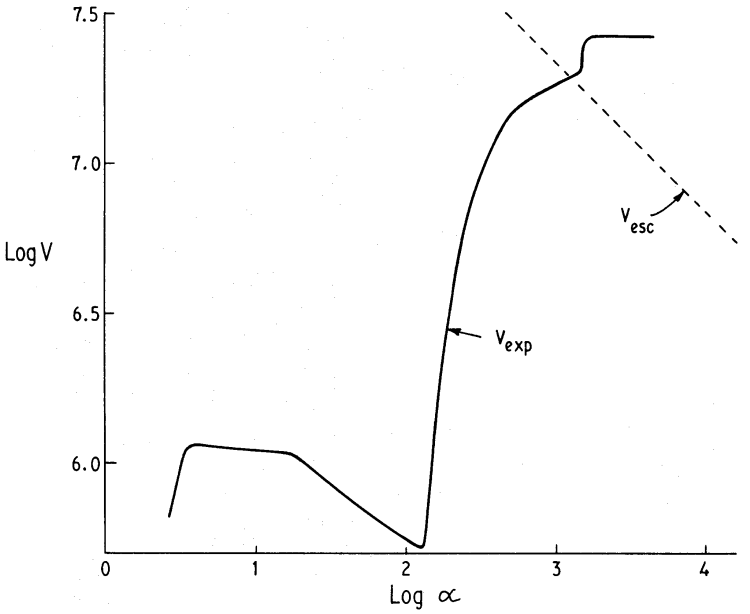

Figure 7. As Fig. 4 but for sequence B.

Although the maximum bolometric luminosity is higher, the maximum visual luminosity attained in sequence B is less than in sequence A because the density of the outflowing material is lower allowing us to see deeper into the star. Hence the photospheric temperature and bolometric correction are higher.

The time for material to flow through the interaction zone is found to be about 5 hr, which is approximately the binary period. To see why this should be so, suppose all the interaction energy goes into driving mass loss from radius S, so that

$$L_D = M_{int}\, \mathscr{E}_{int} \simeq \frac{GM}{S} F \qquad (45)$$

where now F is the mass outflow rate. This implies that $t_{\rm cross}$, the time to cross the interaction zone, is

$$t_{\rm cross} = \frac{M_{\rm int}}{F} = \frac{GM}{S} \cdot \frac{1}{\mathscr{E}_{\rm int}} \simeq P \tag{46}$$

as $R_2 \simeq S$.

Further since $M_{\rm int} \simeq M_{\rm dyn} = L_{\rm ed}/\mathscr{E}_{\rm int}$ we have

$$F \simeq L_{\rm ed} S/GM. \tag{47}$$

For sequence B, this gives $F = 2 \times 10^{-3} M_\odot\,{\rm yr}^{-1}$ which is in good agreement with the mean value found in the numerical calculations, $F = 1.7 \times 10^{-3} M_\odot\,{\rm yr}^{-1}$.

If a steady outflow were set up the time to eject the whole envelope would be

$$t_{\rm ej} = \frac{M_{\rm env}}{F} \simeq \frac{GMM_{\rm env}}{SL_{\rm ed}} \simeq t_{\rm KH}, \tag{48}$$

i.e. the envelope would be ejected on a roughly thermal time-scale, which for sequence B is $\simeq 40$ day. This is much less than the braking time of the secondary

$$t_{\rm b} \equiv \left|\frac{S}{\dot{S}}\right| = \frac{1}{2}\frac{M_1 M_2}{MM_{\rm int}} P \tag{49}$$

$\simeq 50$ yr and hence we are justified in neglecting changes in S.

The crossing time is also given by

$$t_{\rm cross} \simeq 2R_2/\{(V_1 + V_2)/2\} \tag{50}$$

where V_1 and V_2 are the velocities at radii $S - R_2$ and $S + R_2$ respectively. As $V_1 \ll V_2$, we find

$$V_2 \simeq \frac{4R_2}{t_{\rm cross}} \simeq \frac{4R_2}{P} \tag{51}$$

which gives $V_2 \simeq 90\,{\rm km\,s^{-1}}$ for sequence B. As the material flows outward it undergoes further acceleration and reaches a terminal velocity of $V_{\rm exp} = 300\,{\rm km\,s^{-1}}$ (see Fig. 7) which is greater than the escape velocity and comparable to the principal absorption velocities observed in slow novae.

4 Discussion and conclusions

In Table 3 we compare some observed parameters of particular slow and very slow novae with the same parameters taken from the numerical models. $\Delta M_{\rm v}$ is the range of the outburst in magnitudes. For the numerical models we take the minimum absolute magnitude to be that of the discs of old novae, i.e. $M_{\rm v,min} = 4.5$. $t_{\rm rise}$ is the time to rise from minimum to maximum visual magnitude $M_{\rm v,max}$. $V_{\rm exp}$ is the expansion velocity at maximum visual magnitude. For the observed novae it is taken to be the principal absorption velocity. $t_{\rm max}$ is the time for which the very slow novae remain at or near maximum visual magnitude. t_3 is the time the observed novae take to decline 3 mag from maximum. It is not given for the numerical models because the decline stage cannot be followed in a physically realistic manner using the diffusion approximation to radiative transfer.

The light curves for sequences A and B are shown in Figs 8 and 6 respectively. The bolometric corrections determined by Code *et al.* (1976) for main sequence stars have been

Table 3. Comparison of theory and observation.

	Observed novae					Numerical models	
Object	RR Pic	DQ Her	HR Del	RR Tel	RT Ser	Seq. A	Seq. B
ΔM_V (mag)	11.5	13.6	8.5★	9	>4	10.7	10.2
t_{rise} (day)	75★	8	100	200★	40★	36	3.4
$M_{V,max}$ (mag)	−7.4†, −6.1‡	−5.6†, −6.5‡	−5.9‡	−6★§	?	−6.2	−5.7
V_{exp} (km s^{-1})	300	310	200	100¶	40	40	300
t_{max} (day)	–	–	–	1500	5000	>23	–
t_3	150	100	230	1700	>3000	?	?
Binary period (hr)	3.48	4.65	4.08	?	?	–	3.97
Secondary spectrum	?	?	?	M3 III	?	–	M0 V

★Very uncertain; † Nebular expansion (McLaughlin 1960); ‡Rate of decline – luminosity relation; § Comparison with secondary; ¶ 5 yr after initial rise (Thackeray 1977).

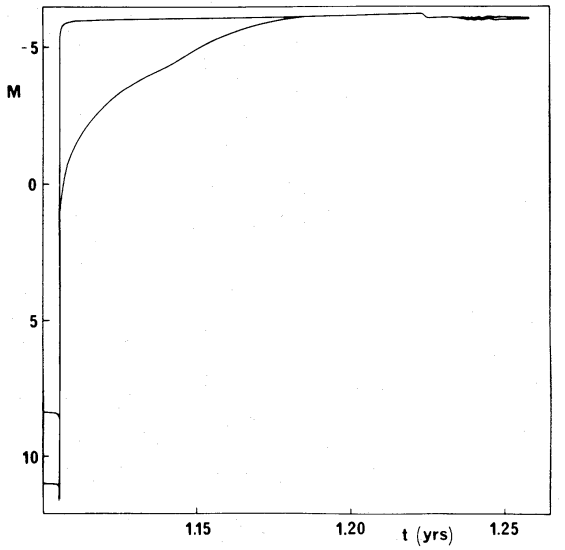

Figure 8. The light curve of sequence A for the total extent of the calculations. The curves are as for Fig. 5.

used, extrapolated when necessary. We note that these are probably too large for extended stars and stars with outflowing envelopes and hence our rise times are probably over-estimates.

We see from Table 3 that the expansion velocity found in sequence A is too low for a slow novae but comparable to the principal absorption velocities of the very slow novae RT Ser and RR Tel. The other parameters of sequence A exhibited in Table 3 are also consistent with the hypothesis that this is a very slow nova outburst. Inclusion of the binary interaction in sequence B increases the expansion velocity to 300 km s^{-1}, a value typical of slow novae such as HR Del, DQ Her and RR Pic. Again the other parameters of sequence B are not inconsistent with the idea that this is a slow nova outburst.

We therefore conclude that thermonuclear runaways on white dwarf stars, in material that contains approximately solar abundances of the CNO nuclei, can give rise to *very slow nova* outbursts if the binary separation is large ($\simeq 10^{13}$ cm) as it must be in RR Tel and RT Ser which have red giant companions detectable in the infrared (Feast & Glass 1974).

Further if the binary separation is small ($\simeq 10^{11}$ cm), as it must be in the short period systems HR Del, RR Pic and DQ Her, dynamic friction between the expanding envelope

and the secondary deposits additional energy into the envelope at a fast enough rate to increase the expansion velocity to a sizable fraction of the orbital velocity. We identify these objects with *slow novae.*

Contrary to the above conclusions, on the basis of a hydrodynamic study of the nova outburst, Prialnik, Shara & Shaviv (1978) have claimed that slow novae can result from unenhanced CNO envelopes. However, their particular model produced expansion velocities of order $10^3 \mathrm{km\,s^{-1}}$ which is much greater than observed (see Table 3). We believe that these high velocities are the result of their treatment of the outer boundary. To simulate mass loss they remove the outermost mass zone of the envelope when its velocity is greater than the local sound speed and the local escape velocity. Despite this condition, a perturbation is transmitted to the interior mass zones (which, presumably, are moving subsonically relative to the removed zone). In particular, the mass zone adjacent to the removed zone will receive an additional outward acceleration because of the sudden, artificial change in pressure gradient (the external pressure was taken to be zero always). It is this non-physical mechanism that maintains the mass loss and, hence, the conclusions of Prialnik *et al.* (1978) are invalid.

A remaining problem with the very slow novae is why t_{max} is so large. Spectroscopic data on RT Ser (Adams & Joy 1928) and RR Tel (Thackeray 1950; Pottasch & Varsavsky 1960) show that, in common with classical novae of all speed classes, emission lines did not appear in any strength until the start of the decline. Hence we have a situation in which there is apparently outflow from a star but no extensive region of optically thin material. As discussed in Section 3, this is possibly due to the outflowing material recombining before attaining escape velocity. A physically and optically thin shell of cool material forms above the photosphere and remains there until it becomes dense enough for gas pressure to continue the expansion (Sparks *et al.* 1978).

It does not seem possible to produce fast novae by the above mechanisms. Furthermore, we do not expect binary interaction to be energetically important in systems in which the principal absorption velocity is appreciably greater than the relative orbital velocity of the two stars, simply because the outflowing material does remain in the vicinity of the binary orbit long enough to be gravitationally influenced by the secondary. Hence the cause of fast nova outbursts must depend on some property of the white dwarf. One possibility that has been investigated in some detail by Starrfield and co-workers (1972, 1974, 1978) is that the CNO abundances in the accreted material are enhanced with respect to the Sun by factors up to 100 by number. Their outbursts reproduce the gross properties of fast novae. Observational evidence for this mechanism is provided by the detection of CNO abundances enhanced by factors 20–100 in the ejecta of the very fast nova V1500 Cygni (Ferland & Shields 1978). However, even greater CNO abundances have also been detected in the nebula of the slow nova DQ Her (Williams *et al.* 1978), an observation that is difficult to reconcile with the theories of Starrfield *et al.*

Acknowledgments

I thank Drs P. P. Eggleton, G. T. Bath, J. E. Pringle and J. Papaloizou for valuable discussions and Professor R. J. Tayler for helpful comments on the manuscript. I acknowledge support from an SRC Studentship.

References

Abramowitz, M. & Stegun, I. A., 1972. *Handbook of Mathematical Functions,* Dover, New York.
Adams, W. S. & Joy, A. H., 1928. *Publs astr. Soc. Pacif.*, **40**, 252.

Baker, N. & Temesvary, S., 1966. *Tables of Convective Stellar Envelope Models,* Goddard Space Flight Center, NASA.
Caughlan, G. R. & Fowler, W. A., 1972. *Nature Phys. Sci.,* **238**, 23.
Code, A. D., Davis, J., Bless, R. C. & Hanbury Brown, R., 1976. *Astrophys. J.,* **203**, 417.
Eggleton, P. P., 1971. *Mon. Not. R. astr. Soc.,* **151**, 351.
Eggleton, P. P., 1972. *Mon. Not. R. astr. Soc.,* **156**, 361.
Eggleton, P. P., Faulkner, J. & Flannery, B. P., 1973. *Astr. Astrophys.,* **23**, 325.
Feast, M. W. & Glass, I. S., 1974. *Mon. Not. R. astr. Soc.,* **167**, 81.
Ferland, G. J. & Shields, G. A., 1978. *Astrophys. J.,* **226**, 172.
Giannone, P. & Weigert, A., 1967. *Z. Astrophys.,* **67**, 41.
Kraft, R. P., 1964. *Astrophys. J.,* **139**, 457.
MacDonald, J., 1979. *PhD thesis,* University of Cambridge.
McLaughlin, D. B., 1960. In *Stars and Stellar Systems,* vol. VI, ed. Greenstein, J. L., University of Chicago Press.
Nariai, K., Nomoto, K. & Sugimoto, D., 1979. Preprint.
Paczynski, B., 1966. *Acta astr.,* **16**, 231.
Paczynski, B., 1976. In *Structure and Evolution of Close Binary Systems*, ed. Eggleton, P., Mitton, S. & Whelan, J., Reidel, Dordrecht, Holland.
Pottasch, S. R. & Varsavsky, C. M., 1960. *Ann. Astrophys.,* **23**, 516.
Prialnik, D., Shara, M. M. & Shaviv, G., 1978. *Astr. Astrophys.,* **62**, 339.
Schwarzschild, M. & Härm, R., 1965. *Astrophys. J.,* **142**, 855.
Sparks, W. M., Starrfield, S. & Truran, J. W., 1978. *Astrophys. J.,* **220**, 1063.
Starrfield, S., Sparks, W. M. & Truran, J. W., 1974. *Astrophys. J. Suppl.,* **28**, 247.
Starrfield, S., Truran, J. W. & Sparks, W. M., 1978. *Astrophys. J.,* **226**, 186.
Starrfield, S., Truran, J. W., Sparks, W. M. & Kutter, S. G., 1972. *Astrophys. J.,* **176**, 169.
Sugimoto, D., 1970. *Astrophys. J.,* **159**, 619.
Thackeray, A. D., 1950. *Mon. Not. R. astr. Soc.,* **110**, 45.
Thackeray, A. D., 1977. *Mem. R. astr. Soc.,* **83**, 1.
Walker, M. F., 1954. *Publs astr. Soc. Pacif.,* **66**, 230.
Williams, R. E., Woolf, N. J., Hege, E. K., Moore, R. L. & Kopriva, D. A., 1978. *Astrophys. J.,* **224**, 171.